

Article

A Shape Optimization Method of a Specified Point Absorber Wave Energy Converter for the South China Sea

Yadong Wen, Weijun Wang * , Hua Liu, Longbo Mao, Hongju Mi, Wenqiang Wang and Guoping Zhang

Department of Electrical Engineering, Army Logistics University of PLA, Chongqing 401331, China; elecivalry@163.com (Y.W.); liuhua6753@163.com (H.L.); mlb84@163.com (L.M.); mimihj_123@163.com (H.M.); 15223330879@163.com (W.W.); zgp064@126.com (G.Z.)

* Correspondence: wjwang636@126.com; Tel.: +86-023-8673-6189

Received: 9 September 2018; Accepted: 30 September 2018; Published: 3 October 2018



Abstract: In this paper, a shape optimization method of a truncated conical point absorber wave energy converter is proposed. This method converts the wave energy absorption efficiency into the matching problem between the wave spectrum of the South China Sea and the buoy's absorption power spectrum. An objective function which combines these two spectra is established to reflect the energy absorbing efficiency. By applying Taguchi design, the frequency domain hydrodynamic analysis and the response surface method (RSM), the radius, cone angle and draft of the buoy are optimized. Since the significant influence of power take-off system (PTO) on energy absorption, the optimal PTO damping under random wave conditions is also studied. The optimal shape is acquired by maximizing the energy absorbing efficiency. Four types of performance and the influence of each geometrical parameter are also obtained. In addition, the cause of the trend of performance as well as the effects of adjusting the input parameters are analyzed. This study can provide guidance for the shape optimization of multi-parameter buoys.

Keywords: wave energy converter; point absorber; shape optimization; Taguchi design; RSM; South China Sea; absorption power spectrum

1. Introduction

In recent decades, in order to obtain wave energy with a high energy density, the development of wave energy converters (WECs) has received increased attention. The first model patent for a WEC was acquired by Girard and his son in 1799 [1]. Since then, thousands of WEC prototypes have been developed, which can be classified into three types according to Falcão [2]: oscillating water column (OWC), overtopping device and oscillating body device. Most WECs are currently in the pre-commercial stage; therefore the major concern at this stage is efficiency and several works have been carried out with respect to design optimization. For example, since physical modelling is widely applied in the optimization of OWC devices, Viviano [3,4] studied the difference between the nonlinear results of small scale model and large scale model, which contributes to correct the scale effect of the results obtained from physical model experiments. Falcão [5] and Gomes [6] concentrate on improving the performance of a floating OWC spar buoy by optimizing the tube geometry and turbine characteristic. As for overtopping devices, Martins [7] performed a numerical study for evaluation of the geometry influence over the dimensionless available power of nearshore overtopping WECs. Han [8] proposed a multi-level breakwater for overtopping wave energy conversion, which optimize the opening width of the lower reservoir, the sloping angle and the height ratio by means of numerical and experimental tests.

As a type of oscillating body device, a point absorber (PA) generally operates in a heave or surge motion to harness wave energy via a buoy, whose diameter is small in comparison to the wavelength.

For the purpose of improving the efficiency of PAs, a few approaches are presented in different energy conversion stages. Usually, PAs can be divided into four stages [9]: the absorption stage, the transmission stage, the generation stage and the conditioning stage. At the energy absorption stage, geometric optimization is usually used to improve the wave energy capture efficiency [10–18]. At the transmission stage, many studies focus on optimizing the PTO system configuration [19–21] and proposing new PTO types for different transmission systems, such as nonlinear power capture mechanism [22,23], fluidic flexible matrix composite PTO pump [24] and gyroscopic PTO [25]. At the generation and conditioning stage, system performance can be improved by optimizing the power conversion quality or applying electrical controllers [26,27].

In addition, due to the randomness and volatility of the wave, control strategies play an important role in the WEC system, which can be applied at multiple stages. Corresponding to the aforementioned three types of approaches, the strategies can be divided into three types as Wang [28] recommended: hydrodynamic control, PTO control and Grid/Load side control. Nowadays many researches focus on latching control [29], declutching control [30], model predictive control [31,32] and so forth.

For the ultimate practical operation of WECs, a precise nonlinear model is imperative. Nonlinear factors, e.g., viscosity, friction, nonlinear wave force and nonlinear PTO system, have received wide attention to improve the reliability of the evaluation results [33,34].

Most of the above approaches are applied to components of WEC, while others focus on the study of wave-to-wire (W2W) models, which take into account all the components, from ocean waves to the electrical network. Through W2W model, designers can simultaneously investigate the coupling relationship between components, improve the overall efficiency and apply advanced control strategies [9,28,35].

The wave energy absorption performance of the buoy has a significant impact on the total efficiency of the PA. Thus, the optimization of the buoy in order to maximize the absorbed wave energy is the first necessary step, which is the focus of this paper. The geometric optimization of traditional marine structures aims to minimize dynamic response to maintain stability [36,37]. Conversely, the geometric optimization of wave energy aims to maximize the dynamic response, thereby improving the energy absorption efficiency [38–41]. In addition, it is well known that, as an input condition for WEC design, sea characteristics directly determine the efficiency and feasibility of WEC. Therefore, a high-performing PA is required to maximize the wave energy absorption based on the sea characteristics of the intended deployment location.

For the purpose of improving the energy absorption efficiency, some studies have been carried out on the optimization of the design of different types of PA in recent years. Based on the sea conditions near the Shetland Islands, McCabe [10,11] used a genetic algorithm to optimize the design of the surging WEC buoy. The WEC shape, parametrically described by bi-cubic B-spline surfaces, was assessed using three cost functions within four different constraint regimes defined by two displacements and two power delivery limits. Under the condition of regular waves, Koh [12] used a multi-objective optimization algorithm to optimize the height and radius of a heave-pitch buoy under the constraint of a cost function. Kurniawan [13] applied a multi-objective algorithm to optimize the size and draft of three pitch buoys under the constraints of two cost functions. Danial Khojasteh [14] and Pastor [15] optimized the radius and draft of hemispherical and conical buoys using Advanced Quantitative Wave Analysis (AQWA) and exhaustive search algorithms based on sea state data from the Iranian coast and the North Sea, respectively. Goggins [16] explored the methodology involved in the shape optimization of several types of heave PAs at the Atlantic marine energy test site. The optimal geometrical configuration was established by defining the significant velocity as the objective function which needed to be maximized. Shami [17] and Shadman [18] used the Design of Experiment (DOE) method to optimize the radius and draft of a heave cylindrical buoy. The objective functions used

are the maximum absorbed power, resonance frequency and absorption bandwidth of the buoy's absorption power spectrum.

In this paper, a geometry optimization methodology for a one-body PA buoy is proposed. Based on the sea characteristics of the South China Sea, the radius, cone angle and draft of the truncated conical buoy are optimized. The optimization process is developed by combining Taguchi design, frequency domain analysis based on linear potential flow theory and the response surface method. The optimization goal is to maximize the energy absorption efficiency. An objective function that relates to the wave spectrum and the absorption power spectrum is established, which also reflects the energy absorption efficiency. Since the solution of wave energy absorption efficiency is deemed as the matching problem between wave spectrum and the absorption power spectrum of buoy, the key step is to acquire these two spectra. According to the joint probability distribution of wave height and period, the wave spectrum is calculated. The absorption power spectrum of each buoy, which relies on hydrodynamic and PTO parameters, is obtained. The PTO system is considered as a pure damping system, and the calculation method of the optimal damping coefficient is determined. The hydrodynamic analysis is conducted by the boundary element software AQWA (19.0, ANSYS, Canonsburg, PA, USA), while the Taguchi design and response surface design are carried out by the statistical analysis software Minitab (17.0, Minitab Inc., Commonwealth, PA, USA); other related calculations are realized by MATLAB (R2010b, The MathWorks, Inc, Natick, MA, USA). The influence of geometric parameters on the results and the reason for the trend of each output parameter are analyzed. The methodology proposed in this paper can be extended to multiple geometric parameters or a multiple-degree buoy optimization process.

This paper is organized as follows, Section 1 gives the introduction. Section 2 describes mathematical model of PA and the establishment of objective function. The geometry optimization methodology is elaborated in Section 3. The calculation of wave spectrum and absorption power spectrum are presented in Sections 4 and 5, respectively. Section 6 analyzes parameter optimization based on RSM. Results and discussions are presented in Section 7. In the end, Section 8 summarizes the conclusion.

2. Theoretical Analysis

The form of WEC considered here is a PA, whose equivalent schematic diagram is shown in Figure 1. F_{wave} denotes the wave exciting force, and m is the mass of buoy. K_{PTO} and R_{PTO} represent the damping and elastic properties of the PTO system, respectively. K is on behalf of the spring characteristics of the hydrostatic force. In this paper, K_{PTO} is ignored since the PTO is deemed as a pure damping system. The PA is considered to be a two-body WEC when the reference is a submerged body but a one-body WEC when the reference is the sea bed, and this paper concentrates on the latter case.

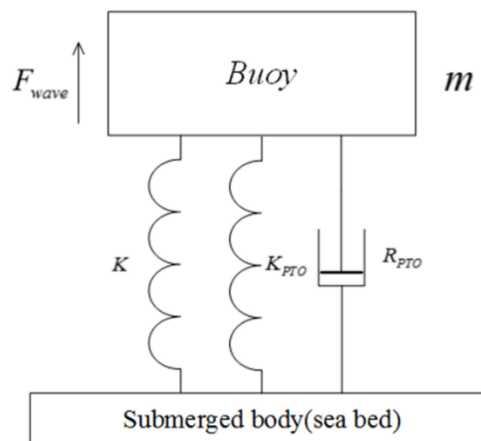


Figure 1. Equivalent schematic diagram of point absorber.

2.1. Mathematical Model

Based on the potential flow theory, buoys are mainly subjected to wave force, hydrostatic restoring force and the force of the PTO system; other external forces such as mooring force are ignored. The external forces cause motion in six degrees of freedom, whereas only heave motion is investigated on account of the fact that wave energy absorption predominately occurs in heave. Ignoring the viscous effects [33,34,40], the force equation of the buoy can be written as

$$m\ddot{z} = f_e + f_r + f_h + f_{ext} = f_e - (A\ddot{z} + B\dot{z}) - \rho gSz + f_{PTO}, \quad (1)$$

where m is the mass of the buoy and z is the dynamic heave motion response. The wave force is composed of the wave excitation force f_e and radiation force f_r . f_r can be expressed as $-A\ddot{z} - B\dot{z}$, where A and B denote the added mass coefficient and radiation damping coefficient, respectively. f_h is the hydrostatic restoring force represented by $-\rho gSz$, S is the buoy's water plane area. For conical buoy, S slightly shifts from the value of stationary state in heave motion. However, in this paper the water plane area is limited to be constant due to insignificant effects. f_{ext} represents the external force, which in the current work is deemed to be equal to the PTO force f_{PTO} .

2.2. Objective Function

In order to optimize the buoy's geometry, an objective function must first be established as the evaluation criteria. In some studies, the energy absorption performance under random wave conditions was evaluated by analyzing the maximum absorbed power, the resonance frequency and the absorption bandwidth (half-power bandwidth). In fact, these three performance parameters are the spectral parameters of the absorption power spectrum of a buoy. The essence of the absorption power spectrum is the dynamic response characteristics of the buoy excited by the incident wave with unit wave amplitude ($a(\omega) = 1$). The energy absorption of the buoy under random spectral conditions can be written as

$$P_R = R_{PTO} \sum_{j=1}^M \omega_j^2 |H(i\omega_j)|^2 S(\omega_j) \Delta\omega, \quad (2)$$

where $H(\omega)$ is the response amplitude operator (RAO), R_{PTO} is the PTO damping coefficient and $S(\omega)$ is the wave spectrum density function. Meanwhile, $a(\omega)$ and $S(\omega)$ have the following relationship:

$$a(\omega) = \sqrt{2S(\omega)\Delta\omega}. \quad (3)$$

Substituting the above equation into Equation (2), the energy absorption at the frequency ω_j may be written as

$$P_R(\omega_j) = \frac{1}{2} R_{PTO} \omega_j^2 |H(i\omega_j)a(\omega_j)|^2 = \frac{1}{2} R_{PTO} \omega_j^2 |H(i\omega_j)|^2. \quad (4)$$

The above formula is the energy absorption spectrum function, which formulates the absorption power spectrum of the buoy. The spectral parameters (resonance frequency, absorption bandwidth and maximum absorbed power) can be obtained by analyzing the spectral characteristics. It is worth noting that the absorption power spectrum is the self-property of the buoy and does not contain sea characteristics. Currently, the main method designs the resonance frequency close to the peak frequency of the target sea state and then maximizes the absorption power and absorption bandwidth. However, this is often faced with the problem of a qualitative trade-off between parameters, which is difficult to quantitatively evaluate. It is the wave spectrum that can fully reflect the energy distribution characteristics of the random spectrum; thus, only analyzing the absorption power spectrum will reduce the reliability under real sea conditions. Hence, it is necessary to establish an objective function that can simultaneously contain information about the energy absorption performance of the buoy and the energy distribution characteristics of the sea state. As Price [42] stated, the absorption power spectrum is similar to a window that captures energy on a wave spectrum. Goggins [16] and Claus [37] suggested using the significant velocity associated with both the dynamic motion response of WEC

and the wave spectrum as the objective function. Referring to the definition of the significant wave height, the significant velocity is defined as

$$V_S^2 = 16 \int_0^\infty S_s(\omega) d\omega, \quad (5)$$

where $S_s(\omega)$ is the dynamic velocity response spectrum and is defined as

$$S_s(\omega) = (|H(i\omega)|\omega)^2 S(\omega). \quad (6)$$

This gives

$$V_S^2 = 16 \int_0^\infty (|H(i\omega)|\omega)^2 S(\omega) d\omega. \quad (7)$$

In discrete form, this becomes

$$V_S^2 = 16 \sum_{j=1}^N (|H(i\omega_j)|\omega_j)^2 S(\omega_j) \Delta\omega. \quad (8)$$

The above equation contains the dynamic response performance of the buoy $|H(i\omega)|\omega|$ and also the information of the wave spectrum ($S(\omega)\Delta\omega$) and so it is more complete than only analyzing the absorption power spectrum. However, it is worth noting that there is no PTO damping parameter in the above equation but it contains the dynamic response $H(i\omega_j)$, which is affected by the PTO damping coefficient. The result is that different results will be obtained under different PTO damping coefficient and it is well known that PTO damping coefficient have a direct impact on the energy absorption, which indicates that using significant velocity as the objective function is still not perfect. Based on this, the objective function proposed in this paper is

$$f = \frac{R_{PTO} V_S^2}{16D}. \quad (9)$$

where D is the waterline diameter. The above equation contains the PTO damping coefficient and the significant velocity, which can compensate for the lack of PTO damping information. Meanwhile, this is also divided by the waterline diameter to help compare the performance of buoys of different sizes.

To fully understand the meaning of the proposed objective function, the following analysis may be conducted. On the one hand, considering Equations (4) and (8), the above equation can be rewritten as

$$f = \frac{R_{PTO} V_S^2}{16D} = \frac{2}{D} \sum_{j=1}^N P_R(\omega_j) S(\omega_j) \Delta\omega_j. \quad (10)$$

It can be seen that the objective function is the sum of the products of the absorption power spectrum and the wave spectrum at each frequency, which means that the degree of matching between the two spectra is reflected.

On the other hand, the relationship between the objective function and the wave energy absorption efficiency may be derived. The absorption efficiency is generally determined by the capture width, which is defined as the ratio of the energy extracted by the buoy to the wave input energy and is given by

$$C_w(\omega) = \frac{R_{PTO} \sum_{j=1}^M \omega_j^2 |H(i\omega_j)|^2 S(\omega_j) \Delta\omega}{\rho g \sum_{j=1}^M v_g(\omega_j, h) S(\omega_j) \Delta\omega_j}, \quad (11)$$

where h is the water depth and v_g is the wave group velocity. Considering Equations (4), (8) and (10), it can be found that

$$C_w(\omega) = \frac{f}{\rho g \sum_{j=1}^M v_g(\omega_j, h) S(\omega_j) \Delta\omega_j} D. \quad (12)$$

According to Cheng [43], the denominator is the wave input energy of the unidirectional long-crested random sea. When the random spectrum is given, its annual average wave input energy is constant and so the objective function is proportional to the capture width when the size is constant, which indicates that the objective function can simultaneously reflect the absorption efficiency under random waves.

Till then, conclusion can be drawn that by establishing the objective function, the wave energy absorption efficiency is converted into the matching problem of the wave energy and absorption power spectrum.

3. Geometry Optimization Methodology

From the established objective function, the key to evaluating the performance of the buoy is to obtain the wave spectrum and the absorption power spectrum. The Taguchi design, hydrodynamic analysis and response surface method (RSM) are combined to achieve optimization. The design flowchart is shown in Figure 2. First, according to the joint probability distribution of significant wave height (SWH) and wave average period (T_{av}), the South China Sea's wave spectrum is obtained. Secondly, given the range of the buoy geometry parameters, the candidate buoy library is obtained by the Taguchi method. Then, the hydrodynamic performance of the candidate buoy is analyzed, along with the optimal PTO damping coefficient of each buoy being calculated to obtain the absorption power spectrum. On the basis of obtaining these two spectra, the objective function is applied to evaluate the performance so as to obtain the approximate range of the optimal buoy parameters. Finally, the RSM is used for local optimization to obtain the optimal buoy parameter configuration.

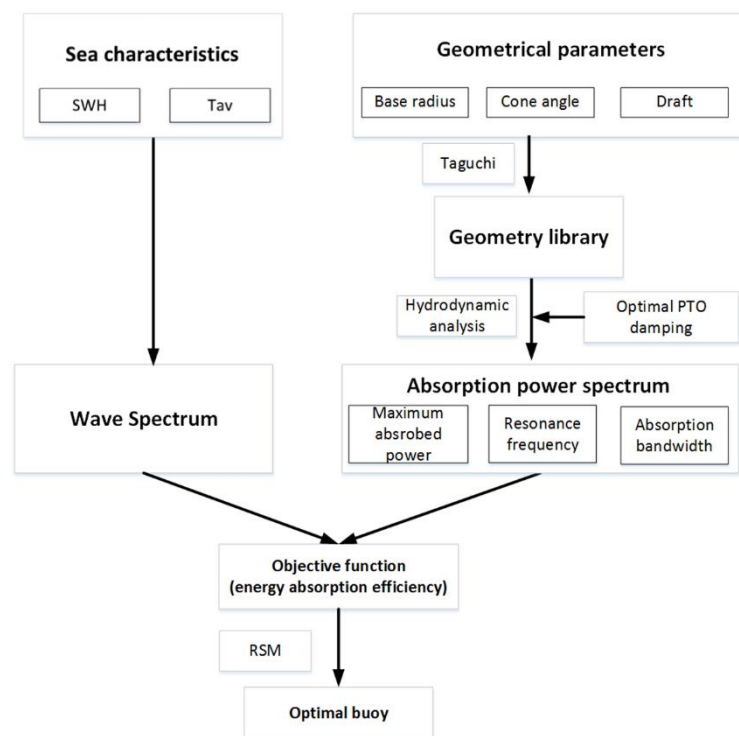


Figure 2. Flowchart of geometrical optimization.

The wave spectrum calculation is presented in Section 4, while the Taguchi design and hydrodynamic analysis are utilized in Section 5 for the sake of calculating absorption power spectrum. The parameter optimization based on RSM is elaborated in Section 6.

4. Wave Spectrum

The purpose of the sea state analysis is to obtain the wave spectrum. The intended deployment site is the South China Sea, which contains a large amount of potential wave energy. Zheng [44,45] has performed a large number of works over the last several years. In one study of his, the wave field in the China Sea from January 1988 to December 2011 was simulated using the WAVEWATCH-III (WW3) model, with a Cross-Calibrated, Multi-Platform (CCMP) wind field as the driving field. The joint probability distributions of average annual significant wave height (SWH) and wave average period (T_{av}) are presented in Table 1. SWH represents the mean wave height of the top one-third of the waves. The background color scale illustrates the occurrence probability level, showing that the most probable SWH values are below 4.5 m and the majority of SWH values fall in the 0.5–2.5 m interval. Most of the wave periods are distributed within the range of 3.5–9.5 s. The wave power level, P , per unit width in a wave can be calculated as follows [46]:

$$P = \frac{\rho g^2 H_s^2 T_{av}}{64\pi}, \tag{13}$$

where ρ is the density of the fluid, g is acceleration due to gravity and H_s and T_{av} denote SWH and average wave peak period, respectively.

Table 1. Joint probability distribution of significant wave height (SWH) and wave average period (T_{av}).

| | | Wave Average Period (s) | | | | | | | | | | | | |
|----------------------------------|------|-------------------------|------|--------|------|------|------|------|-----|------|------|------|------|------|
| | | 1.5 | 3.5 | 4.5 | 5.5 | 6.5 | 7.5 | 8.5 | 9.5 | 10.5 | 11.5 | 12.5 | 13.5 | 14.5 |
| significant wave height (SWH, m) | 10.5 | 0 | 0 | 0 | 0 | 0 | 0 | 0 | 0 | 0 | 0 | 0 | 0 | 0 |
| | 9.5 | 0 | 0 | 0 | 0 | 0 | 0 | 0 | 0 | 0 | 0 | 0 | 0 | 0 |
| | 8.5 | 0 | 0 | 0 | 0 | 0 | 0 | 0 | 0 | 0 | 0 | 0 | 0 | 0 |
| | 7.5 | 0 | 0 | 0 | 0 | 0 | 0 | 0 | 0 | 0 | 0 | 0 | 0 | 0 |
| | 6.5 | 0 | 0 | 0 | 0 | 0 | 0 | 0 | 1 | 9 | 2 | 0 | 0 | 0 |
| | 5.5 | 0 | 0 | 0 | 0 | 0 | 0 | 28 | 54 | 24 | 1 | 0 | 0 | 0 |
| | 4.5 | 0 | 0 | 0 | 0 | 0 | 50 | 373 | 240 | 37 | 7 | 0 | 0 | 0 |
| | 3.5 | 0 | 0 | 0 | 0 | 163 | 1317 | 950 | 436 | 86 | 0 | 0 | 0 | 0 |
| | 2.5 | 0 | 0 | 0 | 874 | 4743 | 2891 | 1459 | 546 | 54 | 0 | 0 | 0 | 0 |
| | 1.5 | 0 | 19 | 3720 | 9300 | 5011 | 2925 | 1131 | 149 | 7 | 1 | 0 | 0 | 0 |
| | 0.5 | 531 | 4859 | 11,299 | 6525 | 3159 | 997 | 189 | 38 | 3 | 2 | 0 | 0 | 0 |

By combining the occurrence probabilities detailed in Table 1 with Equation (13), the wave power level at each sea state is estimated as shown in Table 2. The background color scale illustrates the wave power level. It can be seen that in this sea state, the largest energy contribution is given by waves with an SWH of 2–3 m and a period of 6–7 s, which account for about 15.2% of the energy. The second-largest energy contribution (10.7%) comes from waves with an SWH of 2–3 m and a period of 7–8 s and the third-largest (9.6%) is from waves with an SWH of 3–4 m and a period of 7–8 s. By normalizing the power level of each sea state in Table 2 (divided by the total number of wave occurrences, 64,210), a single equivalent energy distribution can be obtained as shown in Figure 3, from which the resultant annual average energy density is calculated as approximately 10 kW/m. According to Figure 3, the equivalent wave height for each period (frequency) can be obtained by Equation (13) and then the wave spectrum density function, $S(\omega)$, at the period (frequency) can be calculated by Equation (3). After the $S(\omega)$ at each period (frequency) is acquired, the wave energy spectrum of the South China Sea can be obtained by interpolation method, as shown in Figure 4. It is observed that the peak wave angular frequency is 0.837 rad/s (viz. $T_p = 7.5$ s) and the highest wave spectrum density is about 0.83 m²/(rad/s).

Table 2. Wave power level and energy contribution distribution.

| | | Wave Average Period (s) | | | | | | | | | | | | |
|----------------------------------|------|-------------------------|------|--------|--------|--------|--------|--------|--------|------|------|------|------|------|
| | | 1.5 | 3.5 | 4.5 | 5.5 | 6.5 | 7.5 | 8.5 | 9.5 | 10.5 | 11.5 | 12.5 | 13.5 | 14.5 |
| significant wave height (SWH, m) | 10.5 | 0 | 0 | 0 | 0 | 0 | 0 | 0 | 0 | 0 | 0 | 0 | 0 | 0 |
| | 9.5 | 0 | 0 | 0 | 0 | 0 | 0 | 0 | 0 | 0 | 0 | 0 | 0 | 0 |
| | 8.5 | 0 | 0 | 0 | 0 | 0 | 0 | 0 | 0 | 0 | 0 | 0 | 0 | 0 |
| | 7.5 | 0 | 0 | 0 | 0 | 0 | 0 | 0 | 0 | 0 | 0 | 0 | 0 | 0 |
| | 6.5 | 0 | 0 | 0 | 0 | 0 | 0 | 0 | 196 | 1959 | 476 | 0 | 0 | 0 |
| | 5.5 | 0 | 0 | 0 | 0 | 0 | 0 | 3533 | 7616 | 3741 | 170 | 0 | 0 | 0 |
| | 4.5 | 0 | 0 | 0 | 0 | 0 | 3727 | 31,510 | 22,660 | 3861 | 800 | 0 | 0 | 0 |
| | 3.5 | 0 | 0 | 0 | 0 | 6370 | 59,386 | 48,549 | 24,902 | 5429 | 0 | 0 | 0 | 0 |
| | 2.5 | 0 | 0 | 0 | 14,745 | 94,569 | 66,511 | 38,042 | 15,911 | 1739 | 0 | 0 | 0 | 0 |
| | 1.5 | 0 | 74 | 18,486 | 56,485 | 35,969 | 24,226 | 10,616 | 1563 | 81 | 12 | 0 | 0 | 0 |
| | 0.5 | 98 | 2087 | 6239 | 4403 | 2519 | 917 | 197 | 44 | 3 | 2 | 0 | 0 | 0 |

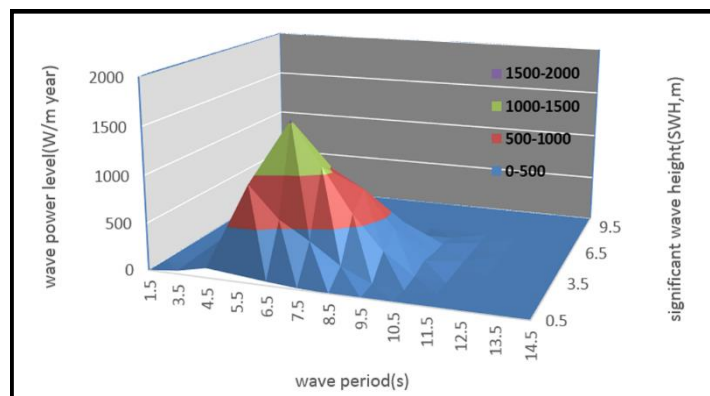


Figure 3. Surface chart of the wave power level for the South China Sea.

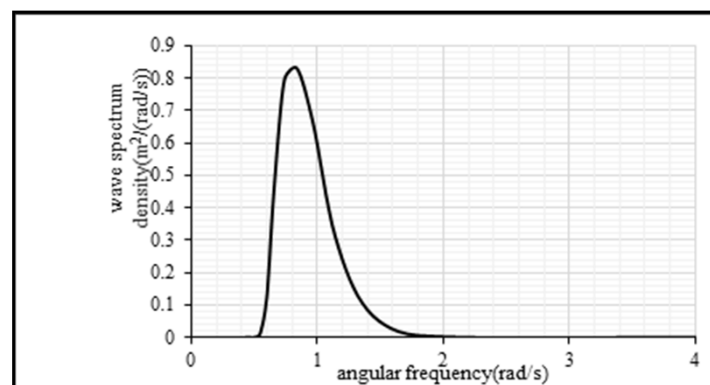


Figure 4. Wave spectrum of the South China Sea.

5. Absorption Power Spectrum

5.1. Geometry Library Generation Based on Taguchi Design

The truncated cone buoy analyzed in this paper is presented in Figure 5, where r is the bottom radius, θ is the cone angle, d stands for the draft and h is the height. Axisymmetric buoys [47] can

accept the energy of any wave direction and can better dissipate the horizontal component of the wave force than other types of buoys, which is beneficial to improving survivability. As one of the axisymmetric buoys, the truncated cone buoy has the advantage of being able to flexibly adjust its waterline area compared to the cylindrical buoy.

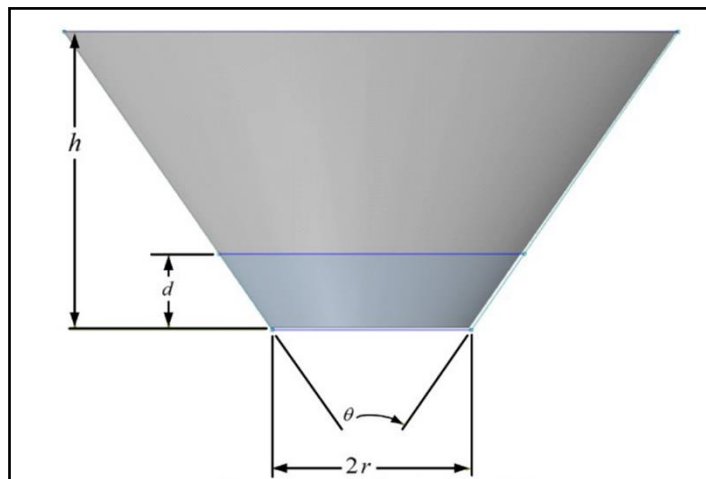


Figure 5. Sketch of the truncated cone buoy.

Taguchi design is an efficient quality management method proposed by Dr. Taguchi in 1950s for optimization of industrial processes. This design approach is based on mathematical statistics and improves product quality/system performance by analyzing the sensitivity of the system response to multiple parameters [48]. The effect of each parameter on the system in Taguchi method is similar to a signal/noise ratio. Taguchi design consists of three sub-designs, namely system design, parametric design and tolerance design. The system design is to determine the technical route or performance parameters used to improve the quality of the product/design; while the parameter design is to determine the optimal level combination of parameters; and the tolerance design is to determine the reasonable tolerance of each parameter, thus achieving the expected quality requirements at the lowest cost.

For the wave energy absorption of PA, corresponding to the system design is to select the truncated cone buoy and determine the three key geometric parameters: base radius, cone angle, draft; corresponding to the parameter design is to determine the optimal level combination of geometric parameters. Since the economic factors are not within the scope of this paper, the tolerance design is not considered at this stage. In addition, Taguchi design can analyze the impact of input parameters on performance to determine the most important parameters and correlation analysis is elaborated in Section 7.2.

The foundation of parameter design is orthogonal arrays, which fulfills the experimental purpose with a minimum number of experiments; it also means that the design is balanced, that is, each parameter is given the same weight. As shown in Figure 5, three parameters which need to be optimized are the base radius (r), cone angle (θ) and draft (d), while the height of the buoy is fixed at three-times the base radius. The range of the geometrical parameters considered in this study is presented in Table 3, in which the draft is considered to be proportional to the base radius.

Table 3. Range of geometrical parameters.

| Geometrical Parameter | Minimum | Maximum |
|-------------------------|---------|---------|
| Base radius (r) | 3 (m) | 12 (m) |
| Cone angle (θ) | 40° | 120° |
| Draft (d) | 0.5 r | 2.5 r |

The above three parameters can be composed into hundreds of buoy shapes within the range of consideration. One feasible method is to take a finite value for each parameter and then combine them into a finite number of buoy representatives. The performance of the buoy representatives is evaluated, while the performance of other shape buoys is obtained by interpolation or fitting. The advantage of this method is that the buoy performance database can be built and the required buoy performance can be conveniently queried during the optimization process but the disadvantage is that the calculation cost is high. Taking five levels for each parameter as an example, up to $5^3 = 125$ tests are required to establish a database. In order to improve the optimization efficiency, Taguchi design is applied in this study. As shown in Table 4, an $L_{25} (5^3)$ orthogonal experiment table is applied and a geometry library which contains 25 buoys is generated.

Table 4. Candidate buoy library.

| Buoy ID | Base Radius (m) | Cone Angle (°) | Draft Ratio (d/r) | CoG (m) | CoB (m) |
|---------|-----------------|----------------|-----------------------|---------|---------|
| 1 | 3 | 40 | 0.5 | −0.9 | −0.7 |
| 2 | 3 | 60 | 1 | −1.8 | −1.28 |
| 3 | 3 | 80 | 1.5 | −2.7 | −1.7 |
| 4 | 3 | 100 | 2 | −3.6 | −2 |
| 5 | 3 | 120 | 2.5 | −4.5 | −2.26 |
| 6 | 6 | 40 | 1 | −3.6 | −2.7 |
| 7 | 6 | 60 | 1.5 | −5.4 | −3.62 |
| 8 | 6 | 80 | 2 | −7.2 | −4.3 |
| 9 | 6 | 100 | 2.5 | −9 | −4.8 |
| 10 | 6 | 120 | 0.5 | −1.8 | −1.2 |
| 11 | 8 | 40 | 1.5 | −7.2 | −5.2 |
| 12 | 8 | 60 | 2 | −9.6 | −6.1 |
| 13 | 8 | 80 | 2.5 | −12 | −6.9 |
| 14 | 8 | 100 | 0.5 | −2.4 | −1.7 |
| 15 | 8 | 120 | 1 | −4.8 | −2.8 |
| 16 | 10 | 40 | 2 | −12 | −8.3 |
| 17 | 10 | 60 | 2.5 | −15 | −9.2 |
| 18 | 10 | 80 | 0.5 | −3 | −2.2 |
| 19 | 10 | 100 | 1 | −6 | −3.8 |
| 20 | 10 | 120 | 1.5 | −9 | −4.9 |
| 21 | 12 | 40 | 2.5 | −18 | −12 |
| 22 | 12 | 60 | 0.5 | −3.6 | −2.8 |
| 23 | 12 | 80 | 1 | −7.2 | −4.9 |
| 24 | 12 | 100 | 1.5 | −10.8 | −6.4 |
| 25 | 12 | 120 | 2 | −14.4 | −7.5 |

In addition, in order to maintain the stability of the buoy and avoid the situation of overturning, the center of gravity (CoG) of buoys are set at 0.6 times the draft under the hydrostatic surface, while the center of Buoyancy (CoB) is calculated by hydrostatic analysis in AQWA. The z coordinates of CoG and CoB are also given in Table 4. It can be seen that all the CoG are located below the CoB, which indicates that all buoys in the library are stable.

5.2. Absorption Power Spectrum Calculation

As can be seen from Equation (4), the absorption power spectrum includes the $H(i\omega)$ term and the PTO damping coefficient term. Among them, $H(i\omega)$ is calculated from the hydrodynamic parameters, so the acquisition of the absorption power spectrum relies on the calculation of hydrodynamic parameters and the PTO damping coefficient.

5.2.1. Hydrodynamic Parameters Calculation

The acquisition of hydrodynamic parameters can be solved by the tank experiment or numerical method and in this paper, the numerical method is applied by using the boundary element software

AQWA. The frequency range of interest is divided into 20 equal parts and the wave excitation force, the added mass and the radiation damping coefficient are obtained under unit wave amplitude condition. The dynamic response $H(i\omega)$ is calculated as

$$H(i\omega) = \frac{z(i\omega)}{a(\omega)} = \frac{f_e(i\omega)}{-(m_1 + A_1)\omega^2 + i\omega(B_1 + R_{PTO}) + (\rho g S + K)}. \quad (14)$$

5.2.2. Optimal PTO Damping Determination

The PTO damping coefficient affects the dynamic response performance of the buoy [49,50]. It is assumed that the PTO system is a pure damping system and the mass and spring properties are neglected [43]. Falnes [51] pointed out that, in a regular wave, the maximum absorbed power is obtained when the PTO damping coefficient is equal to the conjugate of the inherent damping of the system, as follows:

$$R_{PTO} = \sqrt{B_1^2 + (\omega m_1 + \omega A_1 - (\rho g S + K)/\omega)^2}. \quad (15)$$

Price [42] indicates that the optimal damping under random wave conditions should be related to the spectral and buoy characteristics and the best case is that the PTO damping is always equal to the conjugate value of the system impedance; however, this is difficult to achieve in practice. The suboptimal condition used in this paper is that the PTO damping is always equal to the inherent damping of the system at the wave peak frequency. Instead of ω , the peak frequency ω_p of the wave spectrum is used and Equation (15) can be rewritten as

$$R_{PTO} = \sqrt{B_1^2 + (\omega_p m_1 + \omega_p A_1 - (\rho g S + K)/\omega_p)^2}. \quad (16)$$

It should be noted that some research determines the PTO damping coefficient as equal to the radiation damping coefficient. The premise of this optimal PTO damping condition is that the buoy is in a resonance state; that is, the buoy resonance frequency is equal to the peak frequency. In fact, when the buoy is in resonance, the second square term under the root of the equation of the above equation is equal to zero; that is, the PTO damping coefficient is equal to the radiation damping, so the above formula is more universal than the radiation damping condition.

When the optimal damping is determined, the RAO of the buoy can be calculated in MATLAB according to Equation (14) and the absorption power spectrum of each buoy can be obtained according to Equation (4).

6. Parameter Optimization Based on RSM

After obtaining the wave spectrum and the absorption power spectrum, the energy absorption efficiency of each buoy can be evaluated according to the objective function. By evaluating the energy absorption efficiencies of all candidate buoys, the optimal level of the three geometric parameters can be determined. Taguchi design can quickly realize a multi-factor optimization process. The only shortcoming is that it can merely analyze isolated design points and the optimization results are not detailed enough. Compared with Taguchi design, the prediction model obtained by the response surface method (RSM) is continuous, which means that it can continuously analyze input parameters. The RSM method was first introduced by Box and Wilson for modelling, problem analysis development, modification and optimization of various processes [52]. Although other experimental design and optimization methods can find the optimal value, it is difficult for the designer to intuitively discriminate the optimization region due to the lack of the intuitive graph. For this reason, the response surface method has emerged. It takes the response of the system (such as the wave energy absorption performance studied in this paper) as a function of multiple parameters. Since the prediction model is continuous, it can use graphical techniques to display this functional relationship for the designer to select the optimal conditions by intuitive observation.

In addition, when the parameter range is wide, RSM yields to a high calculation cost due to the need of a large number of design points. However, when the parameter range is narrow, an ideal result can be achieved which is suitable for analysis after the Taguchi design result and more accurate results could be obtained. To this end, local response surface optimization is performed near the optimal level obtained by Taguchi design and finally the optimal buoy parameters are obtained.

7. Results and Discussion

According to the proposed optimization method, four types of performance, namely the objective function value, absorption bandwidth, resonance frequency and maximum absorbed power of the buoy, are obtained. First, the optimal geometric parameter configuration is analyzed from two perspectives: energy absorption efficiency (objective function) and absorption power spectrum parameters. Secondly, the magnitude of each geometric parameter's effect on performance parameters (objective function and absorption power spectrum parameters) as well as the cause of the trend of each performance parameter are studied. Then, the control effects of adjusting the geometric parameters and PTO damping are discussed. Finally, based on the results of the Taguchi design, the local response surface optimization is conducted and the final buoy design is obtained.

7.1. Optimal Geometry Configuration Analysis

The main effect diagram of the energy absorption efficiency (objective function), the resonance frequency, the absorption bandwidth and the maximum absorbed power of the buoy are shown in Figures 6–9, respectively. It can be seen from Figure 6 that the energy absorption efficiency shows a trend of increasing first and then decreasing with increasing radius and cone angle and decreasing with the increase of draft. The maximum value is obtained when radius is equal to 6, the cone angle is equal to 60° – 80° and the draft is equal to 0.5.

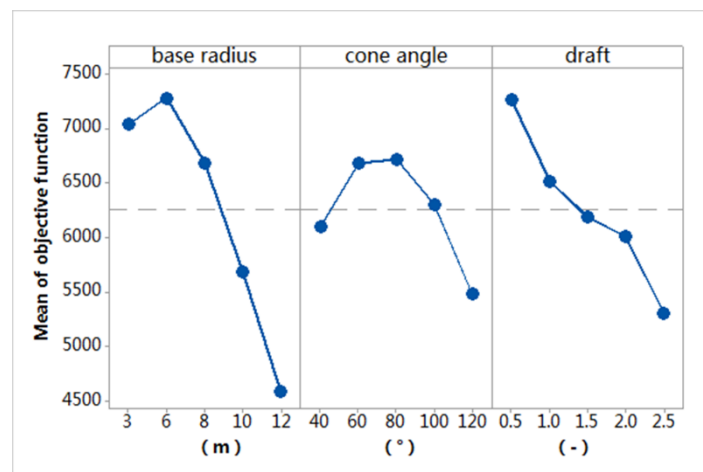


Figure 6. Main effects diagram for objective function.

As seen in Figure 7, the resonance frequency of most of the buoys are lower than the peak frequency of the wave spectrum (0.837 rad/s) and the average resonance frequency of the buoy with a radius of 6, a cone angle of 60° – 80° , or a draft ratio of 0.5 is basically near 0.7 rad/s, which is higher than most other candidate buoys. This result stems from the fact that values shown in the main effect diagram is the average of buoys with the same geometrical parameters. For instance, buoy 6 ($r = 6$, $\theta = 40^{\circ}$, $d/r = 1$) has a resonance frequency of 0.818 rad/s, while buoy 9, with the same radius ($r = 6$, $\theta = 120^{\circ}$, $d/r = 2.5$), has a resonance frequency of 0.57 rad/s.

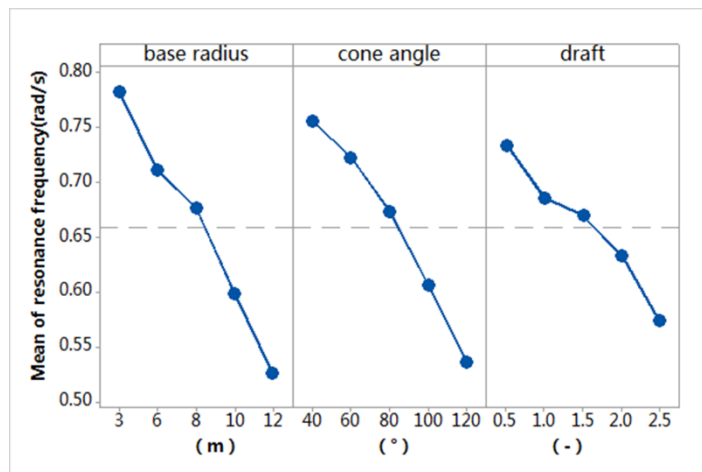


Figure 7. Main effects diagram for resonance frequency.

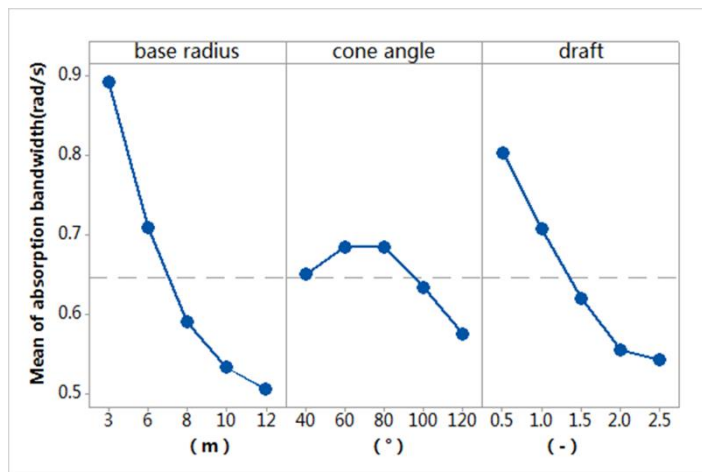


Figure 8. Main effects diagram for absorption bandwidth.

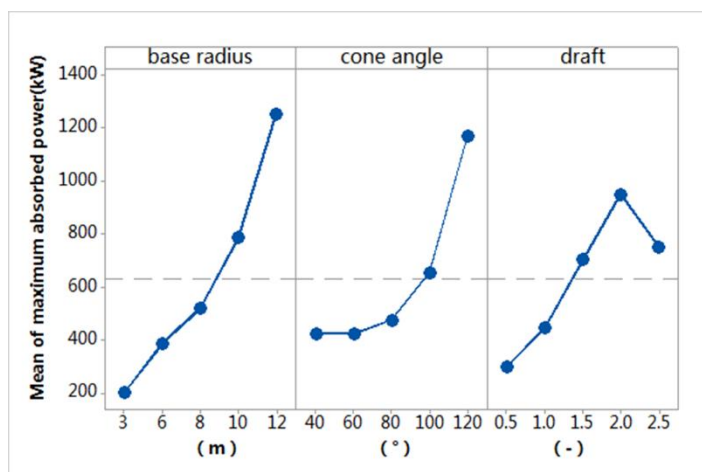


Figure 9. Main effects diagram for maximum absorbed power.

It can be seen from Figure 8 that the absorption bandwidth of the buoy with a cone angle equal to 60°–80° or a draft of 0.5 is optimal. As for the radius, the absorption bandwidth of the buoy with a radius of 6 is next to the buoy with a radius of 3. The bandwidth of the buoy with the above geometric

parameters is in the range of 0.67–0.8 rad/s, which is wider than the bandwidth of the wave spectrum (0.42 rad/s).

Figure 9 shows that the maximum absorbed power of the buoy with a radius of 6, an angle of 60°–80°, or a draft of 0.5 is relatively small. However, as discussed previously, the value of the resonance frequency and the absorption bandwidth for these geometrical parameters is greater, viz., the matching with the wave spectrum is more suitable and therefore the energy absorption efficiency is better. This also shows to some extent that the pursuit of a better match with the wave spectrum is more important than the pursuit of maximum absorbed power. In addition, Figure 9 shows that the maximum absorbed power is obtained at the maximum radius (radius = 12 m), the maximum angle (cone angle = 120°) and the larger draft ratio (draft ratio = 2); however, it can be seen from Figure 6 that the energy absorption efficiency is low when each geometric parameter takes a maximum value. That is to say, the geometric parameters at which the larger maximum absorption power is obtained correspond to lower energy absorption efficiency, which results in high cost and low cost-effectiveness. To this point, the conclusion can be drawn that the optimal geometric parameter levels are a radius equal to 6, a cone angle equal to 60°–80° and a draft ratio equal to 0.5.

Based on the above results, the response surface optimization design is performed. The response surface type adopted is the central composite design (CCD). Since the energy absorption efficiency and the draft are always negatively correlated, the draft is fixed at 0.5 and the performance of the buoy with a radius in the range [6, 8] and angle in the range [60, 80] is optimized. The response surface of the buoy’s objective function with respect to radius and angle is shown in Figure 10 and the response surface optimizer is used to predict the optimal result, as shown in Figure 11. The optimal geometric configuration with a radius of 6.7 m, an angle of 80° and a draft ratio of 0.5 (the draft depth of 3.35 m) is finally obtained.

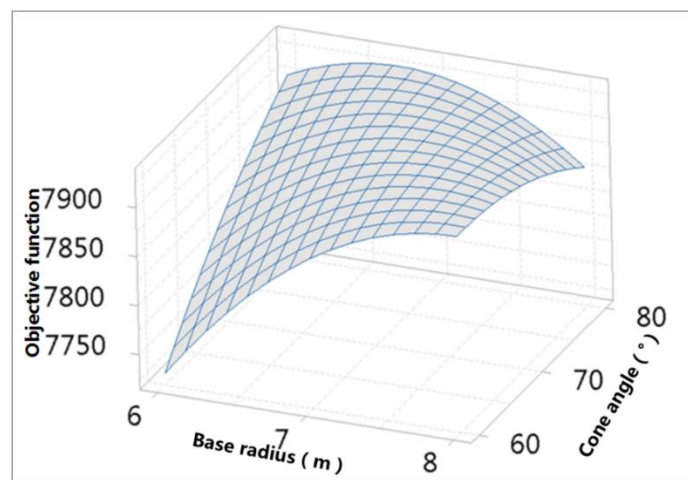


Figure 10. Surface diagram of objective function vs. cone angle and base radius.

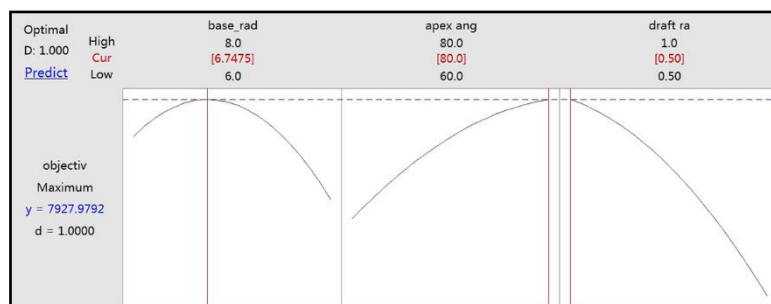


Figure 11. Calculation result of response surface method (RSM) optimizer.

7.2. Performance Characteristic Analysis

7.2.1. Energy Absorption Efficiency

Taguchi design provides range analysis and variance analysis to analyze the influence degree of each geometric parameter on output performance. In this study, the range analysis is adopted due to convenience. It can be seen from Table 5 that the radius has the greatest influence on the energy absorption efficiency, followed by the draft and angle has the least influence.

Table 5. Influence degree of geometric parameters on energy absorption efficiency.

| | Base Radius | Cone Angle | Draft |
|------------|-------------|------------|-------|
| Maximum | 7282 | 6683 | 7264 |
| Minimum | 4591 | 5484 | 5310 |
| Range | 2691 | 1237 | 1954 |
| Percentage | 46% | 21% | 33% |
| Rank | 1 | 3 | 2 |

Furthermore, it was found that the objective function values of all candidate buoys did not exceed 8000, indicating that there is an upper limit to the objective function value. It can be seen from Equation (12) that the objective function is proportional to the capture width when the size is constant. Since the energy capture width of a single-degree-of-freedom axisymmetric buoy has a theoretical maximum of $\lambda/2\pi$ [2], there is also an upper limit to the objective function.

7.2.2. Resonance Frequency

Table 6 illustrates that the radius has the greatest influence on the resonance frequency, followed by the angle and finally the draft.

Table 6. Influence degree of geometric parameters on resonance frequency.

| | Base Radius | Cone Angle | Draft |
|-----------------|-------------|------------|--------|
| Maximum (rad/s) | 0.7820 | 0.7560 | 0.7335 |
| Minimum (rad/s) | 0.5263 | 0.5364 | 0.5735 |
| Range (rad/s) | 0.2557 | 0.2196 | 0.1600 |
| Percentage | 40% | 35% | 25% |
| Rank | 1 | 2 | 3 |

As can be seen from Figure 7, the increase in geometric parameters results in a decrease in the resonance frequency. To analyze the cause of the trend of resonance frequency, the simplified natural frequency formula may be applied, which is written as

$$\omega = 2\pi\sqrt{\frac{\rho g S}{m + A1}}. \quad (17)$$

The increase of geometric parameters will lead to an increase of the mass of the buoy. In addition, the added mass will change accordingly. Taking the radius as an example, the trend of the added mass with the radius is shown in Figure 12. It can be seen that the increase of the radius will lead to an increase in the added mass. The hydrodynamic parameters are closely related to the submerged volume and the increase of the geometric parameters will cause the submerged volume to increase, so the resonance frequency decreases as the geometric parameters increase.

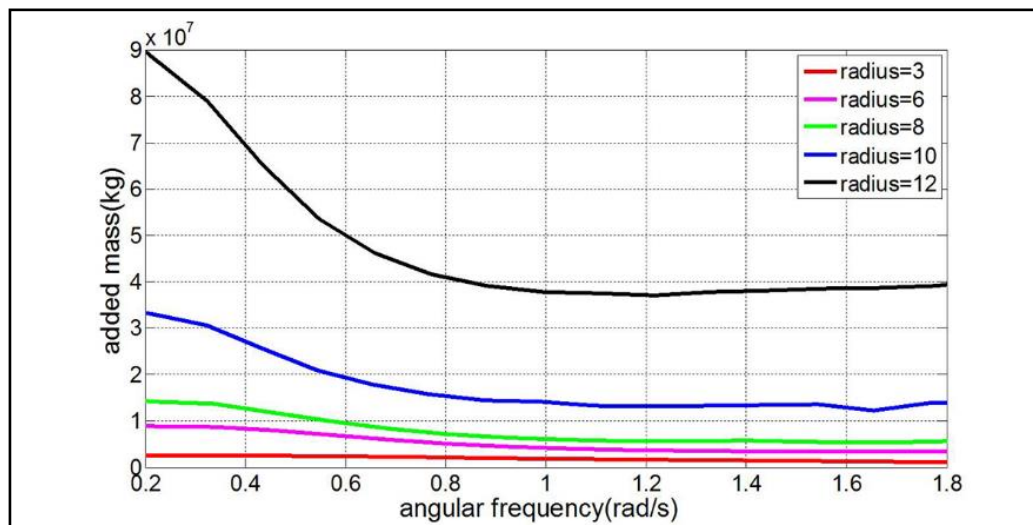


Figure 12. Diagram of added mass vs. base radius.

7.2.3. Absorption Bandwidth

As seen in Figure 8, the absorption bandwidth decreases as the radius and draft increase. As the cone angle changes, the bandwidth tends to become larger and then smaller and the maximum value is obtained at an angle of 60° – 80° . The degree of influence of each geometric parameter on the absorption bandwidth is shown in Table 7, which shows that the radius has the greatest influence, followed by the draft and finally the angle.

Table 7. Degree of influence of geometric parameters on absorption bandwidth.

| | Base Radius | Cone Angle | Draft |
|-----------------|-------------|------------|--------|
| Maximum (rad/s) | 0.8919 | 0.6856 | 0.8039 |
| Minimum (rad/s) | 0.5064 | 0.5762 | 0.5439 |
| Range (rad/s) | 0.3855 | 0.1096 | 0.2600 |
| Percentage | 51% | 15% | 34% |
| Rank | 1 | 3 | 2 |

The absorption bandwidth of a single buoy is related to the damping coefficient of the oscillating system. As a result, for the sake of analyzing the cause of the trend of absorption bandwidth, it is necessary to pay attention to the systematic damping coefficient. According to Falnes [51], the systematic damping coefficient can be calculated as

$$\delta = \frac{R_{pto} + B_1(\omega)}{2(A_1(\omega) + m)}. \quad (18)$$

Taking the hydrodynamic parameters at the peak frequency as representative, the variation of the systematic damping coefficient with respect to the geometric parameters is plotted in Figure 13. As can be seen, when the radius and the draft change, the systematic damping coefficient and the absorption bandwidth change equally and when the cone angle changes, the systematic damping coefficient is opposite to the absorption bandwidth. The reason for this difference may be that the system damping coefficient calculated here ignores the variation of the hydrodynamic coefficient with frequency. In addition, the damping coefficient of the system does not change much under different angles. It is also known from the previous range analysis that the influence of the angle on the bandwidth is only 15% and the impact is minimal.

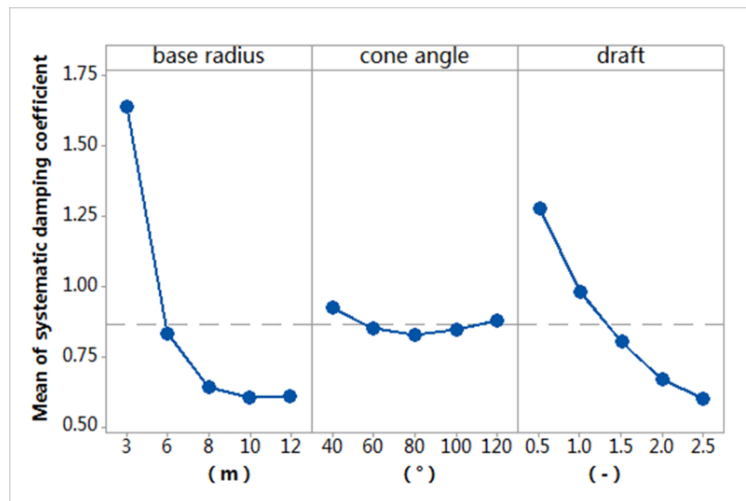


Figure 13. Main effects plot for systematic damping coefficient.

Moreover, Equation (18) indicates that when the geometry of the buoy is specified, the hydrodynamic parameters are also determined and increasing the PTO damping deduces the increase of the absorption bandwidth. Falnes [51] recommended that in order to make the absorption bandwidth larger than the bandwidth of the wave spectrum, R_{PTO} should be greater than the radiation damping. According to Equation (16), the R_{PTO} proposed in this paper is not less than the radiation damping, therefore all candidate buoys have a wider absorption bandwidth than the bandwidth of the wave spectrum (0.42 rad/s).

7.2.4. Maximum Absorbed Power

As can be seen from Figure 9, the maximum absorbed power mostly increases with the increase of the geometrical parameter and decreases only when the draft ratio is 2.5. As shown in Table 8, the radius has the greatest influence, followed by the cone angle and finally the draft ratio.

Table 8. Influence degree of geometric parameters on maximum absorbed power.

| | Base Radius | Cone Angle | Draft |
|--------------|-------------|------------|-------|
| Maximum (kW) | 1254 | 1169 | 951 |
| Minimum (kW) | 201 | 423 | 297 |
| Range (kW) | 1053 | 746 | 654 |
| Percentage | 43% | 30% | 27% |
| Rank | 1 | 2 | 3 |

The energy-absorbing ability of the buoy is attributable to the radiation capability. For the purpose of extracting the incident wave energy as much as possible, a radiation wave field is required to dissipate the incident wave field behind the buoy. The radiation capacity is associated with the radiation damping. To this end, the mathematical relationship between absorbed power and radiation damping coefficient needs to be analyzed. The absorbed power formulated by the hydrodynamic parameters is

$$P_R = \frac{R_{PTO}}{2} |\hat{u}|^2 = \frac{(R_{PTO}/2) |\hat{f}_e|^2}{(B_1 + R_{PTO})^2 + ((m_1 + A_1)\omega - (\rho g S + K)/\omega)^2}. \quad (19)$$

For an axisymmetric buoy with heave motion, the following equation can be obtained by using the Haskind relationship:

$$|f_e|^2 = \frac{4\rho g v_g(\omega, h)}{k} B_1. \quad (20)$$

Substituting Equation (20) into Equation (19) gives

$$P_R = \frac{R_{PTO}}{2} |\hat{u}|^2 = \frac{R_{PTO} B_1 S(\omega_i) \Delta\omega}{(B_1 + R_{PTO})^2 + ((m_1 + A_1)\omega - (\rho g S + K)/\omega)^2} \cdot \frac{4\rho g v_g(\omega, h)}{k}. \quad (21)$$

For the above formula, the partial derivative of the radiation damping B_1 is solved as

$$\frac{\partial P_R}{\partial B_1} = \frac{R_{PTO}^2 + ((m_1 + A_1)\omega - (\rho g S + K)/\omega)^2}{[(B_1 + R_{PTO})^2 + ((m_1 + A_1)\omega - (\rho g S + K)/\omega)^2]^2} \cdot \frac{4R_{PTO}\rho g v_g(\omega, h) S(\omega_i) \Delta\omega}{k} > 0. \quad (22)$$

The above equation illustrates that, with other parameters being constant, the absorbed power is positively correlated with the radiation damping, which is consistent with the study by Babarit [53]. Thus, as can be seen graphically Figures 9 and 14, the relationship between radiation damping at peak frequency and geometric parameters shows that the change trend of the radiation damping is the same as the change trend of the maximum absorbed power.

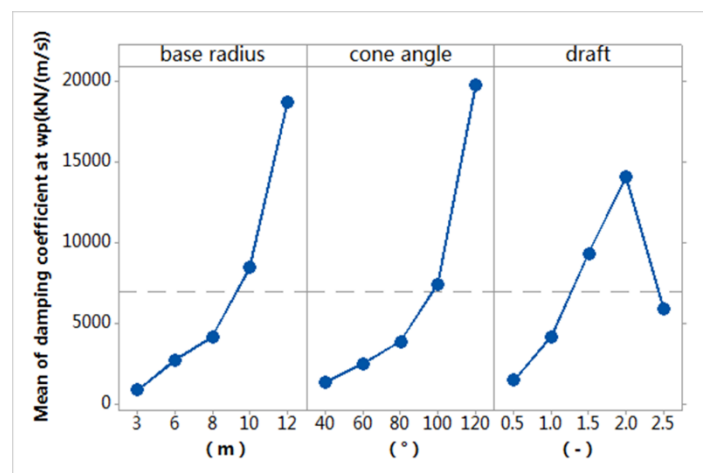


Figure 14. Main effects plot for radiation damping coefficient at peak frequency.

7.2.5. Effects of Adjusting Geometrical Parameters

Studying the relationship between geometric parameters and resonance frequency, the maximum absorbed power and absorption bandwidth are beneficial to guide the optimal process in the future for different target wave conditions. For instance, geometric parameters should be increased to achieve a reduction in the resonance frequency in the case of a lower peak frequency of the wave spectrum. When the wave bandwidth becomes wider, such as from the Joint North Sea Wave Project (JONSWAP) spectrum to the PM spectrum, then the decrease of radius and draft should be considered. The radius and cone angle changes by changing the geometry of the buoy, while changes in draft can be changed by water injection or drainage to change mass. In addition, according to the degree of influence of the geometric parameters analyzed previously on the energy absorption efficiency, the adjustment of radius should be first considered due to its having the greatest impact.

7.2.6. Effects of Adjusting PTO Damping

PTO damping directly affects the absorption performance of the buoy. Taking buoys 6, 7 and 8 as examples, the absorption power spectra under three kinds of PTO damping conditions (100 kNs/m, optimal damping condition and three-times optimal damping) are obtained, as shown in Figure 15.

The wave spectrum is drawn simultaneously and the absorbed power of each buoy is normalized (divided by the maximum absorbed power of buoy 8, viz., 654 kW) for comparison. It can be seen that as the PTO damping increases, the absorption power spectra of buoys shift to the low frequency and the peak values increase. As for spectral parameters, the maximum absorbed power increases with the increase of PTO damping. The resonance frequency decreases as the PTO damping increases, which is inconsistent with the PTO-independent resonance frequency obtained by Equation (17). This inconsistency may be caused by an inconsistent solving method. The former is calculated by the first-order natural frequency formula of solid-state physics, which ignores the change of hydrodynamic parameters with frequency, while the latter is acquired according to the characteristics of the absorption power spectrum, which is related to PTO damping. Besides this, the change of hydrodynamic parameters with frequency is also considered during the calculation process of the absorption power spectrum. As for the absorption bandwidth, it increases with the increase of the PTO damping. To analyze the cause of the trend of the absorption bandwidth, attention need to be paid to Equation (18). It can be seen that the increase of the PTO damping coefficient leads to the increase of the systematic damping coefficient and finally results in the increase of the absorption bandwidth. A larger bandwidth contributes to a reduced need for control strategies.

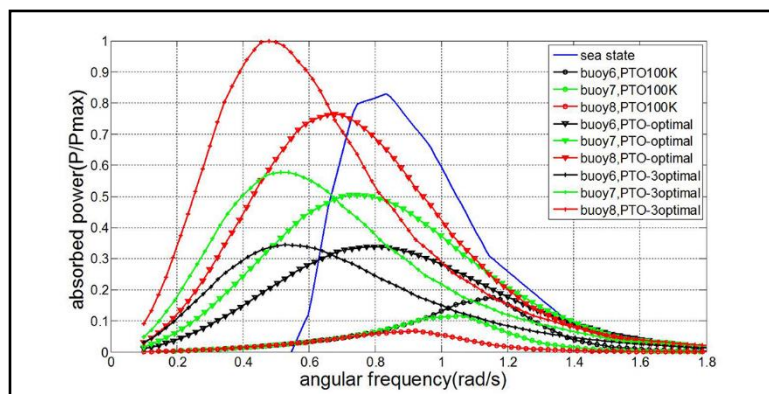


Figure 15. Absorption power spectrum with different power take-off system (PTO) dampings.

8. Conclusions

In this paper, a geometrical optimization method is proposed for a truncated cone buoy of a one-body point absorber wave energy converter. The geometric parameters studied are the radius, cone angle and draft. An objective function, which converts the wave energy absorption efficiency into the matching problem between the wave spectrum and the buoy's absorption power spectrum, is established. The goal of the optimization is to maximize the wave energy absorption efficiency. First, the wave spectrum of the South China Sea was drawn based on sea state data over the past 23 years. Secondly, in order to obtain the buoy absorption power spectrum, the Taguchi design method is applied to generate a buoy library containing 25 candidates. The hydrodynamic parameters are calculated by using the boundary element software AQWA through frequency domain analysis. The PTO system is treated as a pure damping system and the determination of optimal PTO damping is given. According to the hydrodynamic parameters and PTO damping, the absorption power spectrum of each buoy is calculated in MATLAB and the spectral parameters such as resonance frequency, absorption bandwidth and maximum absorbed power are obtained. By analyzing the objective function value and the absorption power spectral parameters, a radius of 6, a cone angle of 60° – 80° and a draft ratio of 0.5 are identified as optimal parameter levels. Then, the response surface method was used for detailed optimization and ultimately a buoy with a radius of 6.7 m, a cone angle of 80° and a draft depth of 3.35 m (draft ratio = 0.5) is deemed as optimal. Finally, the influence magnitude of each geometric parameter's effect on the performance of the buoy, as well as the cause of the trend of performance, is studied. Through the range analysis, the radius has the greatest impact on performance

and the effects of cone angle and draft vary with performance. In addition, the derivation shows that the resonance frequency is related to the mass, the added mass and the PTO damping; the absorption bandwidth is related to the systematic damping coefficient; the maximum absorbed power is related to the radiation damping. This paper reveals the relationship between and the wave spectrum, the energy absorption spectrum of the buoy and the energy absorption efficiency. The proposed method can quickly achieve shape optimization with limited calculations. Furthermore, the effects of viscosity and control strategies should be considered in the future.

Author Contributions: Y.W. and H.L. designed the main parts of the research, including objective function establishment and optimal methodology designing. W.W. (Weijun Wang) was responsible for guidance, a number of key suggestions and manuscript editing. L.M. and H.M. mainly contributed to the writing of the paper and also responsible for project administration. W.W. (Wenqiang Wang) and G.Z. made contributions to simulations in AQWA and gave the final approval of the version to be published.

Funding: This research received no external funding.

Acknowledgments: The authors would like to acknowledge the financial support from “The National Science and Technology Support Program (supported by the Ministry of Science and Technology of P.R.C. No. 2014BAC01B05).” The authors are grateful that comments and suggestions provided by the anonymous reviewers and editor helped to improve the quality of the paper.

Conflicts of Interest: The authors declare no conflict of interest.

References

1. Clément, A.; McCullen, P.; Falcão, A. Wave energy in Europe: Current status and perspectives. *Renew. Sustain. Energy Rev.* **2002**, *6*, 405–431. [[CrossRef](#)]
2. Falcão, F.D.O. Wave energy utilization: A review of the technologies. *Renew. Sustain. Energy Rev.* **2010**, *14*, 899–918. [[CrossRef](#)]
3. Viviano, A.; Naty, S.; Foti, E. Scale effects in physical modelling of a generalized OWC. *Ocean Eng.* **2018**, *162*, 248–258. [[CrossRef](#)]
4. Naty, S.; Viviano, A.; Foti, E. Feasibility study of a WEC integrated in the port of Giardini Naxos, Italy. *Coast. Eng. Proc.* **2017**, *1*, 22. [[CrossRef](#)]
5. Falcão, A.F.O.; Henriques, J.C.C.; Cândido, J.J. Dynamics and optimization of the OWC spar buoy wave energy converter. *Renew. Energy* **2012**, *48*, 369–381. [[CrossRef](#)]
6. Gomes, R.P.F.; Henriques, J.C.C.; Gato, L.M.C. IPS 2Body Wave Energy Converter: Acceleration Tube Optimization. *Int. J. Offshore Polar Eng.* **2010**, *20*, 247–255.
7. Martins, J.C.; Goulart, M.M.; Gomes, M.D.N. Geometric evaluation of the main operational principle of an overtopping wave energy converter by means of Constructal Design. *Renew. Energy* **2018**, *118*, 727–741. [[CrossRef](#)]
8. Han, Z.; Liu, Z.; Shi, H. Numerical study on overtopping performance of a multi-level breakwater for wave energy conversion. *Ocean Eng.* **2018**, *150*, 94–101. [[CrossRef](#)]
9. Penalba, M.; Ringwood, J.V. A Review of Wave-to-Wire Models for Wave Energy Converters. *Energies* **2016**, *9*, 506. [[CrossRef](#)]
10. McCabe, A.P.; Aggidis, G.A.; Widden, M.B. Optimizing the shape of a surge-and-pitch wave energy collector using a genetic algorithm. *Renew. Energy* **2010**, *35*, 2767–2775. [[CrossRef](#)]
11. McCabe, A.P. Constrained optimization of the shape of a wave energy collector by genetic algorithm. *Renew. Energy* **2013**, *51*, 274–284. [[CrossRef](#)]
12. Koh, H.J.; Ruy, W.S.; Cho, I.H. Multi-objective optimum design of a buoy for the resonant-type wave energy converter. *J. Mar. Sci. Technol.* **2015**, *20*, 53–63. [[CrossRef](#)]
13. Kurniawan, A.; Moan, T. Optimal Geometries for Wave Absorbers Oscillating About a Fixed Axis. *IEEE J. Ocean. Eng.* **2013**, *38*, 117–130. [[CrossRef](#)]
14. Khojasteh, D.; Kamali, R. Evaluation of wave energy absorption by heaving point absorbers at various hot spots in Iran seas. *Energy* **2016**, *109*, 629–640. [[CrossRef](#)]
15. Liu, Y.; Pastor, J. Power Absorption Modeling and Optimization of a Point Absorbing Wave Energy Converter Using Numerical Method. *J. Energy Resour. Technol.* **2014**, *136*, 119–129.

16. Goggins, J.; Finnegan, W. Shape optimisation of floating wave energy converters for a specified wave energy spectrum. *Renew. Energy* **2014**, *71*, 208–220. [[CrossRef](#)]
17. Shami, E.A.; Wang, X.; Zhang, R. A parameter study and optimization of two body wave energy converters. *Renew. Energy* **2019**, *131*, 1–13. [[CrossRef](#)]
18. Shadman, M.; Estefen, S.F.; Rodriguez, C.A. A geometrical optimization method applied to a heaving point absorber wave energy converter. *Renew. Energy* **2018**, *115*, 533–546. [[CrossRef](#)]
19. López, M.; Taveira-Pinto, F.; Rosa-Santos, P. Influence of the power take-off characteristics on the performance of CECO wave energy converter. *Energy* **2017**, *120*, 686–697. [[CrossRef](#)]
20. Kim, B.H.; Wata, J.; Zullah, M.A. Numerical and experimental studies on the PTO system of a novel floating wave energy converter. *Renew. Energy* **2015**, *79*, 111–121. [[CrossRef](#)]
21. Gaspar, J.F.; Calvário, M.; Kamarlouei, M.; Soares, C.G. Design tradeoffs of an oil-hydraulic Power Take-Off for Wave Energy Converters. *Renew. Energy* **2018**, *129*, 245–259. [[CrossRef](#)]
22. Zhang, X.; Yang, J. Power capture performance of an oscillating-body WEC with nonlinear snap through PTO systems in irregular waves. *Appl. Ocean Res.* **2015**, *52*, 261–273. [[CrossRef](#)]
23. Zhang, X.; Tian, X.; Xiao, L.; Li, X.; Chen, L. Application of an adaptive bistable power capture mechanism to a point absorber wave energy converter. *Appl. Energy* **2018**, *228*, 450–467. [[CrossRef](#)]
24. Philena, M.; Squibb, C.; Groo, L.; Hagerman, G. Wave energy conversion using fluidic flexible matrix composite power take-off pumps. *Energy Convers. Manag.* **2018**, *171*, 1773–1786. [[CrossRef](#)]
25. Zhang, Z.; Chen, B.; Nielsen, S.R.K.; Olsen, J. Gyroscopic power take-off wave energy point absorber in irregular sea states. *Ocean Eng.* **2017**, *143*, 113–124. [[CrossRef](#)]
26. Hong, Y.; Waters, R.; Boström, C. Review on electrical control strategies for wave energy converting systems. *Renew. Sustain. Energy Rev.* **2014**, *31*, 329–342. [[CrossRef](#)]
27. Ahmed, T.; Nishida, K.; Nakaoka, M. Grid power integration technologies for offshore ocean wave energy. In Proceedings of the Energy Conversion Congress and Exposition, Atlanta, GA, USA, 12–16 September 2010; pp. 2378–2385.
28. Wang, L.; Isberg, J.; Tedeschi, E. Review of control strategies for wave energy conversion systems and their validation: The wave-to-wire approach. *Renew. Sustain. Energy Rev.* **2018**, *81*, 366–379. [[CrossRef](#)]
29. Wu, J.; Yao, Y.; Zhou, L.; Göteman, M. Real-time latching control strategies for the solo Duck wave energy converter in irregular waves. *Appl. Energy* **2018**, *222*, 717–728. [[CrossRef](#)]
30. Zhang, X.T.; Yang, J.M.; Xiao, L.F. Declutching control of a point absorber with direct linear electric PTO systems. *Ocean Syst. Eng.* **2014**, *4*, 63–82. [[CrossRef](#)]
31. Li, G.; Belmont, M.R. Model predictive control of sea wave energy converters—Part I: A convex approach for the case of a single device. *Renew. Energy* **2014**, *69*, 453–463. [[CrossRef](#)]
32. Jama, M.; Wahyudie, A.; Noura, H. Robust predictive control for heaving wave energy converters. *Control Eng. Pract.* **2018**, *77*, 138–149. [[CrossRef](#)]
33. Retes, M.P.; Giorgi, G.; Ringwood, J.V. A Review of Non-Linear Approaches for Wave Energy Converter Modelling. In Proceedings of the 11th European Wave and Tidal Energy Conference, Nantes, France, 6–11 September 2015.
34. Bhinder, M.; Babarit, A.; Gentaz, L. Assessment of viscous damping via 3D-CFD modelling of a Floating Wave Energy Device. In Proceedings of the 9th European Wave and Tidal Energy Conference (EWTEC), Southampton, UK, 5–9 September 2011.
35. Bailey, H.; Robertson, B.R.D.; Buckham, B.J. Wave-to-wire simulation of a floating oscillating water column wave energy converter. *Ocean Eng.* **2016**, *125*, 248–260. [[CrossRef](#)]
36. Birk, L. Application of Constraint Multi-Objective Optimization to the Design of Offshore Structure Hulls. *J. Offshore Mech. Arct. Eng.* **2009**, *131*, 403–410. [[CrossRef](#)]
37. Clauss, G.F.; Birk, L. Hydrodynamic shape optimization of large offshore structures. *Appl. Ocean Res.* **1996**, *18*, 157–171. [[CrossRef](#)]
38. Li, H. Ocean Wave Energy Converters: Status and Challenges. *Energies* **2018**, *11*, 1250.
39. Devolder, B.; Stratigaki, V.; Troch, P. CFD Simulations of Floating Point Absorber Wave Energy Converter Arrays Subjected to Regular Waves. *Energies* **2018**, *11*, 641. [[CrossRef](#)]
40. Zurkinden, A.S.; Ferri, F.; Beatty, S. Non-linear numerical modeling and experimental testing of a point absorber wave energy converter. *Ocean Eng.* **2014**, *78*, 11–21. [[CrossRef](#)]

41. Piscopo, V.; Benassai, G.; Cozzolino, L. A new optimization procedure of heaving point absorber hydrodynamic performances. *Ocean Eng.* **2016**, *116*, 242–259. [[CrossRef](#)]
42. Price, A.A.E.; Dent, C.J.; Wallace, A.R. On the capture width of wave energy converters. *Appl. Ocean Res.* **2009**, *31*, 251–259. [[CrossRef](#)]
43. Cheng, Z.S.; Yang, J.M.; Hu, Z.Q. Frequency/time domain modeling of a direct drive point absorber wave energy converter. *Sci. China Phys. Mech.* **2014**, *57*, 311–320. [[CrossRef](#)]
44. Zheng, C.W.; Zhuang, H.; Li, X. Wind energy and wave energy resources assessment in the East China Sea and South China Sea. *Sci. China Technol. Sci.* **2012**, *55*, 163–173. [[CrossRef](#)]
45. Zheng, C.W.; Pan, J.; Li, J.X. Assessing the China Sea wind energy and wave energy resources from 1988 to 2009. *Ocean Eng.* **2013**, *65*, 39–48. [[CrossRef](#)]
46. Falnes, J. A review of wave-energy extraction. *Mar. Struct.* **2007**, *20*, 185–201. [[CrossRef](#)]
47. Shi, H.; Cao, F.; Liu, Z. Theoretical study on the power take-off estimation of heaving buoy wave energy converter. *Renew. Energy* **2016**, *86*, 441–448. [[CrossRef](#)]
48. Taguchi, G.; Cariapa, V. Taguchi on Robust Technology Development: Bringing. *J. Press. Vess.-Technol. Asme* **1993**, *115*, 161–171. [[CrossRef](#)]
49. Hansen, A.H.; Asmussen, M.F.; Bech, M. Model Predictive Control of a Wave Energy Converter with Discrete Fluid Power Power Take-Off System. *Energies* **2018**, *11*, 635.
50. Beatty, S.; Ferri, F.; Bocking, B. Power Take-Off Simulation for Scale Model Testing of Wave Energy Converters. *Energies* **2017**, *10*, 973. [[CrossRef](#)]
51. Falnes, J. *Ocean Waves and Oscillating Systems: Linear Interactions Including Wave-Energy Extraction*; Cambridge University: Cambridge, UK, 2002.
52. Verma, P.; Sharma, M.P.; Dwivedi, G. Prospects of bio-based alcohols for Karanja biodiesel production: An optimisation study by Response Surface Methodology. *Fuel* **2016**, *183*, 185–194. [[CrossRef](#)]
53. Babarit, A. A database of capture width ratio of wave energy converters. *Renew. Energy* **2015**, *80*, 610–628. [[CrossRef](#)]



© 2018 by the authors. Licensee MDPI, Basel, Switzerland. This article is an open access article distributed under the terms and conditions of the Creative Commons Attribution (CC BY) license (<http://creativecommons.org/licenses/by/4.0/>).